NREL
NATIONAL RENEWABLE ENERGY LABORATORY

Imaging Study of Multi-Crystalline Silicon Wafers Throughout the Manufacturing Process

Preprint

Steve Johnston, Fei Yan,
and Mowafak Al-Jassim
National Renewable Energy Laboratory

Katherine Zaunbrecher
National Renewable Energy Laboratory and Colorado State University

Omar Sidelkheir and Alain Blosse
Calisolar

Presented at the 37th IEEE Photovoltaic Specialists Conference (PVSC 37)
Seattle, Washington
June 19-24, 2011

Conference Paper
NREL/CP-5200-50724
July 2011

Contract No. DE-AC36-08GO28308

Available electronically at http://www.osti.gov/bridge

Available for a processing fee to U.S. Department of Energy
and its contractors, in paper, from:

U.S. Department of Energy
Office of Scientific and Technical Information

P.O. Box 62
Oak Ridge, TN 37831-0062
phone: 865.576.8401
fax: 865.576.5728
email: mailto:reports@adonis.osti.gov

Available for sale to the public, in paper, from:

U.S. Department of Commerce
National Technical Information Service
5285 Port Royal Road
Springfield, VA 22161
phone: 800.553.6847
fax: 703.605.6900
email: orders@ntis.fedworld.gov
online ordering: http://www.ntis.gov/help/ordermethods.aspx

Cover Photos: (left to right) PIX 16416, PIX 17423, PIX 16560, PIX 17613, PIX 17436, PIX 17721

Printed on paper containing at least 50% wastepaper, including 10% post consumer waste.

IMAGING STUDY OF MULTI-CRYSTALLINE SILICON WAFERS THROUGHOUT THE MANUFACTURING PROCESS

Steve Johnston[1], Fei Yan[1], Katherine Zaunbrecher[1,2], Mowafak Al-Jassim[1], Omar Sidelkheir[3], and Alain Blosse[3]
[1]National Renewable Energy Laboratory, Golden, CO, USA
[2]Colorado State University, Fort Collins, CO, USA
[3]Calisolar, Sunnyvale, CA, USA

ABSTRACT

Imaging techniques are applied to multi-crystalline silicon bricks, wafers at various process steps, and finished solar cells. Photoluminescence (PL) imaging is used to characterize defects and material quality on bricks and wafers. Defect regions within the wafers are influenced by brick position within an ingot and height within the brick. The defect areas in as-cut wafers are compared to imaging results from reverse-bias electroluminescence and dark lock-in thermography and cell parameters of near-neighbor finished cells. Defect areas are also characterized by defect band emissions. The defect areas measured by these techniques on as-cut wafers are shown to correlate to finished cell performance.

INTRODUCTION

Imaging techniques can rapidly characterize material quality and defect density. Photoluminescence (PL) imaging can be applied to silicon from the brick level to all wafer process steps. [1-8] At the brick level, material thickness allows for measurement and correlation to lifetime where surface recombination effects are minimized. [6,7] At the as-cut wafer level where thin unpassivated wafers prevent accurate lifetime assessment due to surfaces, defects can still be categorized and quantified to predict finished cell performance. [3-5] Defect regions can be identified by recombination-limited band-to-band PL or by defect-band emission. [9,10]

EXPERIMENT

Band-to-band PL imaging is collected using a Princeton Instruments Pixis 1024BR Si CCD camera cooled to about -50°C. The light source is composed of four 810-nm laser diodes with engineered diffusers to spread out the light over the sample. The intensity is near that of one sun, or ~100 mW/cm^2. As shown in Fig. 1, we have collected PL images on multi-crystalline silicon bricks. The bricks are 156 mm wide and about 28 cm tall, and we have taken two one-megapixel images and stitched them together. These images of the front and back faces show some non-uniformities in the excitation and camera lens that lead to artifacts of bright areas in the center of each half and some bright streaks from the corners toward the center. A line scan of each image is shown in the plots of Fig. 1, where PL intensity is seen to decrease at the bottom and top regions.

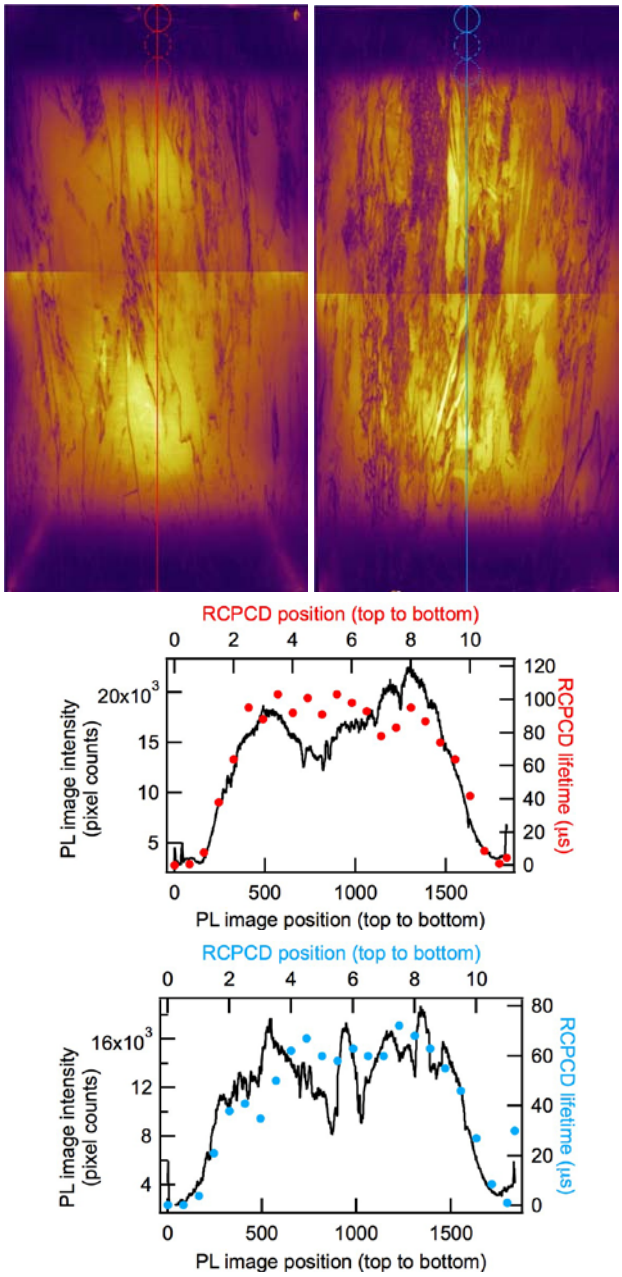

Figure 1 Top images are PL images of the front and back sides of a brick. The plots show a line scan down the center of each face comparing PL intensity to lifetime.

Resonant-coupled photoconductive decay (RCPCD) is a transient-decay minority-carrier lifetime measurement technique. [11] Using ~12-mm-diameter spot size of 1150-nm excitation laser pulses (5 ns pulsewidth), we have measured lifetimes along the same center line of each side. In Fig. 1, the circles on the PL images show the relative spot size and how the spot is stepped along the entire length of the brick. The lifetimes are then plotted on the right axis in comparison with the PL intensity to show a correlation. This correlation could then transform the PL image into a high-resolution lifetime map. [6,7]

For cast multi-crystalline silicon ingots, the defect structure in the form of grain boundaries and dislocation clusters typically increases with brick height from bottom to top. The PL images on as-cut wafers from various heights within a corner brick and interior brick are shown in Fig. 2. The image position corresponds with brick position, i.e., the bottom images are from the bottom of the bricks, and top images are from the top of the bricks.

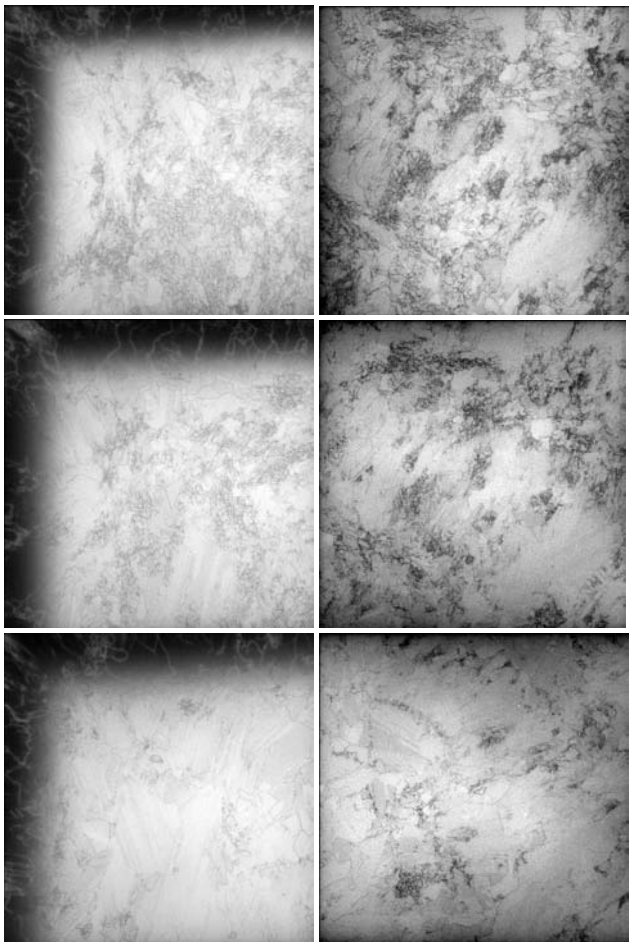

Figure 2 Examples of defect density increasing with brick height for a corner brick (left) and interior brick (right). The bottom images are from the bottom of the bricks, while the middle and top images are of wafers from the middle and top of the bricks.

PL imaging can be measured on wafers at all steps of the solar cell manufacturing process. Thin wafers with unpassivated surfaces do not allow for accurate measurement of bulk minority-carrier lifetime. [4,5,7] At the early process steps, such as after wire sawing and saw-damage removal and texturing, the lifetime is dominated by surface recombination. Long lifetime regions are limited by surface recombination such that average material quality cannot be distinguished from very good material quality. However, defect areas appear dark in PL images due to their short lifetime and high recombination, and these defect areas often are the cell's limiting performance regions as seen by quantum efficiency and light beam induced current maps on finished cells. Consequently, even though PL imaging on as-cut wafers may not give quantitative values of lifetime and an accurate assessment of bulk material quality, it can still be used to detect and characterize defect areas that do correlate to finished cell performance. [3-5]

Neighboring wafers have been processed through a manufacturing line with removal of wafers at each step to show how PL imaging varies by process. These steps include wafer sawing, cleaning and texturing, emitter diffusion, edge isolation and phosphosilicate glass (PSG) removal, anti-reflective coating (ARC) and passivation, and metallization of finished cells. Figure 3 shows examples of PL imaging on neighboring wafers from the middle regions of both a corner brick (left column) and an interior brick (right column).

As-cut wafers are challenging to image due to high surface recombination, but identifying highly defective wafers at this early process step may have the largest savings impact if such wafers are determined to be too poor and not worth processing. Wafers could also be categorized by defect level so that high-quality wafers could be processed on a manufacturing line to take full advantage of their potential efficiency, while defect-containing wafers may benefit from modified processing to enhance cell performance. [3,5] Examples of defects seen by PL imaging on as-cut wafers are shown in the top images of Fig. 3.

While texturing doesn't appear to affect the PL image, the diffusion process of forming the junction does significantly alter the PL image. Contrast between defect-containing and relatively defect-free regions is greatly enhanced. When the thermally-grown PSG is removed in the subsequent etch step, the image contrast is slightly reduced, suggesting that some additional surface passivation was provided by the PSG. Also in the pre-diffusion images for the corner wafer, the crucible-related impurities dominate the dark defect regions of these wafers, but after diffusion, impurity gettering appears to have effectively reduced the relative defect level of the edges compared to grain boundaries and dislocation clusters within the wafer. The ARC processing doesn't appear to significantly alter the PL image when compared to the etching step after diffusion.

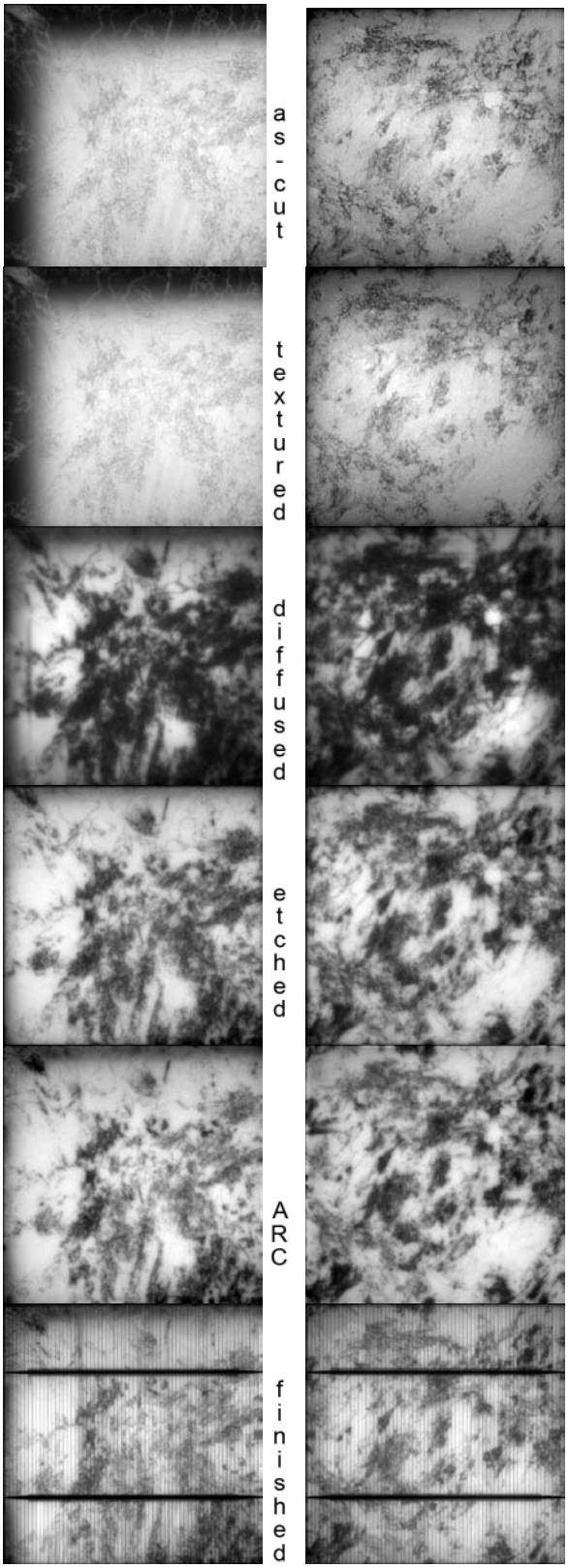

Figure 3 PL imaging of near neighbor wafers at all process steps for a corner brick and interior brick.

Metallization and the associated firing that can release defect-passivating hydrogen from the silicon-nitride ARC layer may lead to subtle improvements in reduced defect contrast, but overall, the defect areas in the finished cells appear quite similar to those in the etched step and even in the as-cut wafer, away from the crucible edges. With the knowledge that defects in as-cut wafers persist through to completed cells, we can attempt to form a correlation of defect regions on as-cut wafers to final cell performance. [3-5] Corner and edge wafers contain crucible-contaminated borders that have less impact on cell performance than they appear to at the as-cut stage. These areas are thus highlighted and counted separately as shown in Fig. 4.

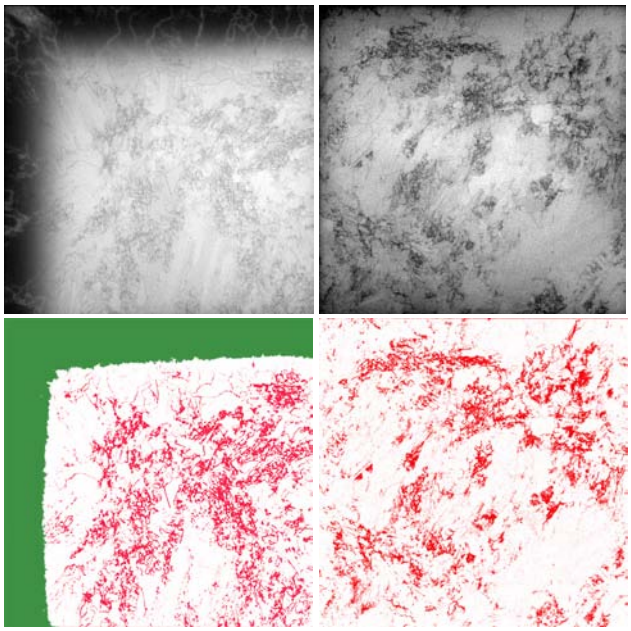

Figure 4 PL images of corner-brick and interior-brick wafers are shown in the top row. Below each PL image is a defect-highlighted image for that wafer.

For the corner wafer, an image threshold level is defined that highlights the dark impurity region, which is shown in green. For the remaining area, and for the entire wafer for those from interior bricks, another threshold is defined to highlight grain boundaries and dislocation/defect clusters, which are shown in red. Each is then summed to give a defect area fraction of the wafer.

Weighting factors are assigned so that the red-colored defects due to dislocations and grain boundaries are weighed more heavily than the green-colored impurity areas at the wafer edges. A linear combination of these defect area fractions forms a total defect parameter. This defect parameter from as-cut wafers is plotted in Fig. 5 to compare to near-neighbor finished cell efficiency, open-circuit voltage (V_{OC}), and short-circuit current (J_{SC}). The blue and purple markers correspond to wafers and cells from corner bricks, while the orange markers represent wafers and cells from an interior brick. Correlations

between the as-cut wafers' defect parameter and the finished cells' efficiency, V_{OC}, and J_{SC} are evident.

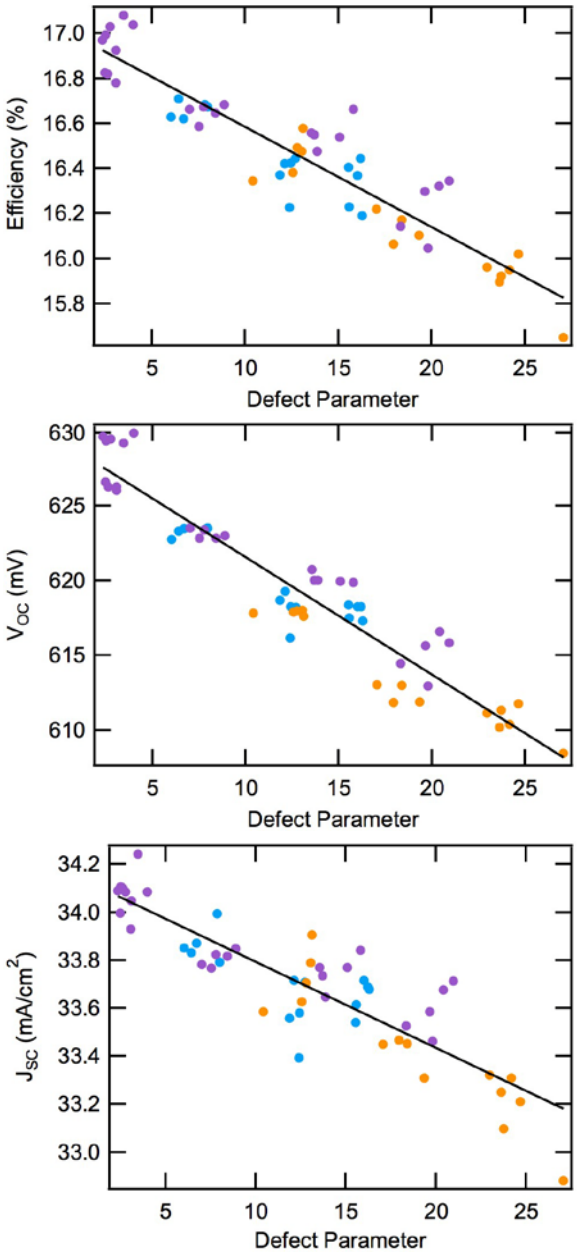

Figure 5 Defect parameter of as-cut wafers compared to finished cell performance. Blue and purple markers represent wafers and cells from corner bricks, and orange markers represent an interior brick.

Imaging techniques requiring contacts can be applied to finished cells. These techniques include electro-luminescence (EL) and dark lock-in thermography (DLIT). [12-16] Examples of these techniques applied to the finished cells of Fig. 3 are shown in Fig. 6. Forward bias EL images are shown in the top row, and they appear quite similar to the PL images of Fig. 3. Resistance issues such as firing non-uniformities or broken grid lines can often show up as differences between EL and PL images, but none appear obvious in this case.

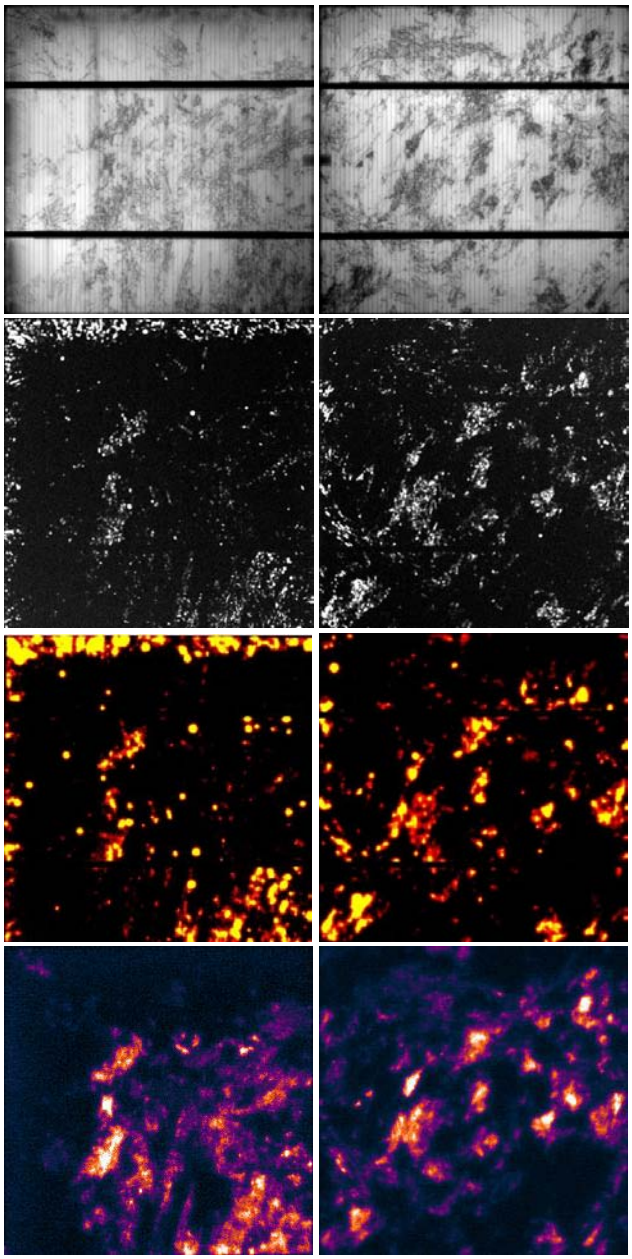

Figure 6 EL images of the finished cells of Fig. 3. The top row shows forward bias, while the second row shows ReBEL imaging with a reverse bias of 12 V. The third row shows DLIT also using 12 V_{rev}. The bottom row shows defect band emission on corresponding near-neighbor as-cut wafers.

The second row of images in Fig. 6 shows Reverse-Bias EL (ReBEL) images at 12 V_{rev}. [17-19] Visible light emits from regions where diode breakdown is occurring. The pattern of breakdown occurring at defect areas compares

well to the DLIT images shown in the third row of Fig. 6. The DLIT images are also collected using a reverse bias of 12 V.

Defect states in silicon can emit radiative sub-bandgap photons. [9,10] We have used a FLIR SC2500 InGaAs camera with sensitivity to detect photons with wavelengths from 0.9 to 1.7 μm. This spectrum covers both the silicon band-to-band emission at ~1.1 eV (1150 nm) and defect-related emission at ~0.8–1.0 eV (1250–1550 nm). For defect band emission imaging, a long-pass filter with a cut-off wavelength at 1350 nm is used to block band-to-band PL. The camera contains a lock-in detection option to improve the signal-to-noise ratio. Defect band PL is collected when pulsing the 810-nm laser diode excitation at about 7 Hz. Examples of the resulting defect band PL are shown in the bottom row of Fig. 6, where bright regions correspond to strong defect band emission. These defect band areas compare well to those where diode breakdown occurs in reverse bias and those where PL and EL images are dark due to high recombination. Defect band emission is suppressed in the areas of high impurity contamination from the ingot crucible, as seen for the corner as-cut wafer in the bottom left image of Fig. 6. [10] As shown with the band-to-band PL images, this edge area improves with processing, so defect characterization with this sub-bandgap PL can still correlate to finished cell device performance. The defect band emission is quantified for each as-cut wafer by setting a threshold value. Then, the area fraction of intensities above this threshold is plotted against finished cell efficiency, V_{OC}, and J_{SC} in Fig. 7. Similar to Fig. 5, the blue and purple markers represent wafers and cells from corner bricks, and orange markers represent an interior brick. Also similar to the band-to-band PL image analysis, correlations between the as-cut wafers' defect band emissions and the finished cells' efficiency, V_{OC}, and J_{SC} are evident.

SUMMARY

We have shown that PL imaging can be measured on silicon bricks and at every step of processing into solar cells. PL images on silicon bricks can be correlated to lifetime and could be used for high-resolution analysis and characterization. PL images at process steps show defect areas and how some evolve with processing while many detrimental areas remain from as-cut to finished cells. Such defect areas can be quantified and correlated to cell performance so that as-cut wafers could be classified to their potential for cell efficiency before processing. Reverse-bias breakdown imaging was collected using both reverse-bias EL and dark lock-in thermography. These techniques were shown to also highlight defect areas similar to the high recombination areas seen by PL. Lastly, defect band imaging using an InGaAs camera was shown, and correlations of these defect areas seen on as-cut wafers also correlated to finished cell parameters.

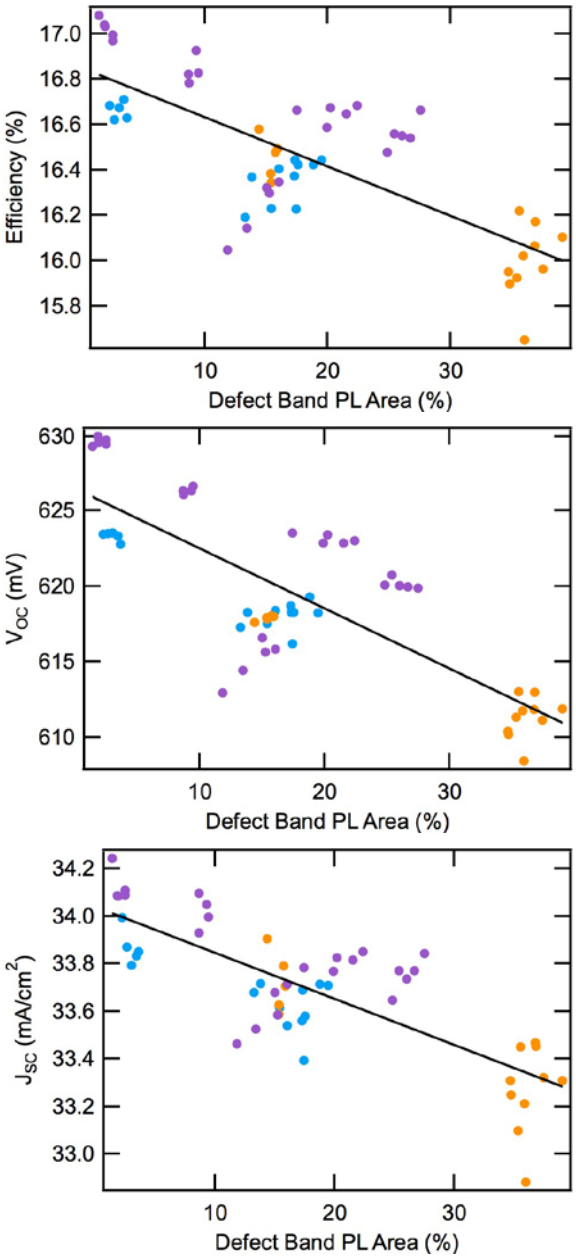

Figure 7 Defect band emission PL of as-cut wafers correlated to near-neighbor finished cell performance. Blue and purple markers represent wafers and cells from corner bricks, and orange markers represent an interior brick.

ACKNOWLEDGEMENT

This work was supported by the U.S. Department of Energy under Contract No. DE-AC36-08GO28308 with the National Renewable Energy Laboratory and with support from the American Recovery and Reinvestment Act.

REFERENCES

[1] T. Trupke, R. A. Bardos, M. C. Schubert, and W. Warta, “Photoluminescence Imaging of Silicon Wafers”, *Appl. Phys. Lett.* **89**, 2006, 044107.

[2] T. Trupke, R. A. Bardos, M. D. Abbott, F. W. Chen, J. E. Cotter, and A. Lorenz, “Fast Photoluminescence Imaging of Silicon Wafers”, *32nd IEEE PVSC* and *WCPEC-4*, 2006, pp. 928-931.

[3] W. McMillan, T. Trupke, J. W. Weber, M. Wagner, U. Mareck, Y. C. Chou, and J. Wong, “In-line Monitoring of Electrical Wafer Quality Using Photoluminescence Imaging”, 25th EPVSEC/5th WCPEC, Valencia, Spain, 2010, pp. 1346-1351.

[4] J. Haunschild, M. Glatthaar, M. Demant, J. Nievendick, M. Motzko, S. Rein, and E. R. Weber, “Quality control of as-cut multicrystalline silicon wafers using photoluminescence imaging for solar cell production”, Sol. Ener. Mat. & Sol. Cells 94, 2010, pp. 2007-2012.

[5] T. Trupke, J. Nyhus, and J. Haunschild, “Luminescence imaging for inline characterization in silicon photovoltaics”, Phys. Status Solidi RRL **5**, 2011, pp. 131-137.

[6] T. Trupke, J. Nyhus, R. A. Sinton, and J. W. Weber, “Photoluminescence imaging on silicon bricks”, Proceedings of the 24th European Photovoltaic Solar Energy Conference, Hamburg, Germany, 2009, pp. 1029-1033.

[7] B. Mitchell, T. Trupke, J. W. Weber, and J. Nyhus, “Bulk minority carrier lifetimes and doping of silicon bricks from photoluminescence intensity ratios”, J. Appl. Phys. **109**, 2011, 083111.

[8] J. Haunschild, M. Glatthaar, S. Riepe, and S. Rein, “Quality control using luminescence imaging in production of mc-silicon solar cells from UMG feedstock”, 35th IEEE PVSC, 2010, pp. 812-816.

[9] I. Tarasov, S. Ostapenko, C. Haessler, and E. U. Reisner, "Spatially resolved defect diagnostics in multicrystalline silicon for solar cells," Mat. Sci. & Engr. B **71** (1-3), 51-55 (2000).

[10] M. Kittler, W. Seifert, T. Arguirov, I. Tarasov, and S. Ostapenko, “Room-temperature luminescence and electron-beam-induced current (EBIC) recombination behaviour of crystal defects in multicrystalline silicon”, Sol. Ener. Mat. & Sol. Cells **72**, 2002, pp. 465-472.

[11] R. K. Ahrenkiel and S. Johnston, “Contactless measurement of recombination lifetime in photovoltaic materials”, Sol. Ener. Mat. & Sol. Cells **55**, 1998, pp. 59-73.

[12] T. Fuyuki, H. Kondo, T. Yamazaki, Y. Takahashi, and Y. Uraoka, “Photographic Surveying of Minority Carrier Diffusion Length in Polycrystalline Silicon Solar Cells by Electroluminescence”, *Appl. Phys. Lett.* **86**, 2005, 262108.

[13] T. Fuyuki, H. Kondo, Y. Kaji, A. Ogane, and Y Takahashi, “Analytic Findings in the Electroluminescence Characterization of Crystalline Silicon Solar Cells”, *J. Appl. Phys.* **101**, 2007, 023711.

[14] O. Breitenstein, M. Langenkamp, O. Lang, and A. Schirrmacher, “Shunts Due to Laser Scribing of Solar Cells Evaluated by Highly Sensitive Lock-in Thermography”, *Sol. Ener. Mat. & Sol. Cells* **65**, 2001, pp. 55-62.

[15] O. Breitenstein, J. Bauer, J.-M. Wagner, and A. Lotnyk, “Imaging Physical Parameters of Pre-Breakdown Sites by Lock-in Thermography Techniques”, Prog. Photovolt: Res. Appl. **16**, 2008, pp. 679-685.

[16] O. Breitenstein, W. Warta, and M. Langenkamp, “Lock-in Thermography: Basics and Use for Evaluating Electronic Devices and Materials”, 2nd Ed., Springer-Verlag, Berlin, 2010.

[17] A. G. Chynoweth and K. G. McKay, “Photon Emission from Avalanche Breakdown in Silicon”, *Physical Review* **102**, 1956, pp. 369-376.

[18] M. Morschbach, M. Oehme, and E. Kasper, “Visible Light Emission by a Reverse-Biased Integrated Silicon Diode”, *IEEE Trans. Elec. Dev.* **54**, 2007, pp. 1091-1094.

[19] D. Lausch, K. Petter, H. von Wenckstern, and M. Grundmann, “Correlation of Pre-Breakdown Sites and Bulk Defects in Multicrystalline Silicon Solar Cells”, *Phys. Status Solidi RRL* **3**, 2009, pp. 70-72.